IET Generation, Transmission & Distribution

Research Article

Low DC voltage PV generation system with power factor correction and harmonic suppression capability in a distribution network

ISSN 1751-8687
Received on 22nd March 2018
Revised 24th October 2018
Accepted on 18th January 2019
E-First on 25th March 2019
doi: 10.1049/iet-gtd.2018.5144
www.ietdl.org

Tao Ye[1], NingYi Dai[2,3] ✉, Keng Weng Lao[2], Chi-Seng Lam[2,4,5], Man-Chung Wong[2,3]
[1]*Wuhan Guide Infrared Co. Ltd., WuHan, People's Republic of China*
[2]*Department of Electrical and Computer Engineering, University of Macau, Macau, People's Republic of China*
[3]*State Key Laboratory of Internet of Things for Smart City, University of Macau, Macau, People's Republic of China*
[4]*State Key Laboratory of Analog and Mixed Signal VLSI, University of Macau, Macau, People's Republic of China*
[5]*Institute of Microelectronics, University of Macau, Macau, People's Republic of China*
✉ *E-mail: nydai@umac.mo*

Abstract: Building-integrated photovoltaics (PVs) is one of the most promising and elegant ways of producing on-site electricity. The compact and cost-effective PV integration system needs to be developed to convert dc voltage into ac compatible with the grid. A single-stage PV inverter is proposed, and its design and control system implementation are focused on. The proposed system is able to transfer active power to the grid with maximum power point tracking. At the same time, the PV inverter can control reactive power and suppress harmonics due to non-linear loads. By coupling to grid via a series LC branch, the proposed system operates on a dc bus voltage much lower than that of the conventional PV inverter, so that less PV panels need to be connected in series. Therefore, the proposed system is a low-cost and multi-functional alternative to PV inverters in building-integrated applications. Simulation and experimental results are provided to validate its effectiveness.

1 Introduction

Photovoltaic (PV) is an elegant means of producing electricity on site, directly from the sun. At present, the PV power generation system for buildings has reached widespread commercialisation. PV materials are used to replace conventional building materials in parts of the building envelope such as roof and skylights. However, its output power varies with operation conditions such as irradiance, temperature, and shading [1–3].

A majority of building-integrated PV (BIPV) systems are integrated to a distribution network in a nearby switch room. Loads are supplied from the same ac bus where PV generators are connected. The widespread use of energy saving lamps and adjustable speed driver increases the harmonic distortion level in a building distribution network. In Macau, the portion of reactive energy that exceeds 60% of active energy in the same tariff period is charged [4]. Therefore, including reactive power and harmonic conditioning function is important for designing an inverter for a BIPV system.

Power conversion part for a BIPV system can be a single-stage converter or a two-stage converter [5, 6]. A two-stage converter is applicable to PV panels of different capacity and connection. Its first stage regulates the dc voltage and tracks the maximum power of PV panels, while the second stage converts the dc voltage into ac compatible with the grid [7–9]. In comparison, a single-stage converter is able to regulate the dc voltage, achieve maximum power point tracking (MPPT) and power conversion by using less components [10, 11]. Its conversion efficiency is also higher. However, the output voltage of PV panels has to be high enough for a single-stage converter, since it only has limited dc voltage regulation capability without a dc–dc conversion stage.

The system configuration of a typical single-phase single-stage PV inverter is shown in Fig. 1*a* [12, 13]. The inverter is coupled to the point of common coupling (PCC) via an LCL filer, so that high-frequency switching currents are not injected to the distribution system. Moreover, there is an increasing concern about reactive power conditioning and harmonics suppression in the distribution system. A multi-functional PV inverter is more preferable, especially for building-integrated projects [14–16].

Many previous studies have been performed on controlling LCL-coupling inverters. Multi-proportional-resonant (PR) controllers are added to the current control loop of an LCL-coupling inverter for mitigating harmonics effectively [17, 18]. As a result, the complexity of the control method is increased. Moreover, the LCL filter may suffer high-frequency resonance due to the interaction between its capacitor and the equivalent inductor in the weak network. It is therefore important to apply passive or active damping methods [19]. The former one increases system losses, while the latter one increases control complexity [13, 19, 20].

The system configuration of an LC-coupling inverter is shown in Fig. 1*b*. Its series LC branch behaves as inductive units in the high-frequency range. Therefore, high-frequency resonance is not possible to happen. This inverter even can be used as an active damper for suppressing high-frequency resonances in a multi-converter power grid [21]. Previous studies reveal that the LC-coupling inverter is able to operate with its dc-link voltage much lower than the voltage at PCC when its output active and reactive power fall in a certain range [22, 23].

As a result, a LC-coupling inverter is a promising solution for the BIPV system. First, its low dc-link voltage requires less PV panels to be connected in series. It is well known that the output power of a PV array is more prone to partial shading effect if a large number of panels are in series [3, 24]. Although a two or multi-stage PV converter can also reduce the dc-link voltage, a less component converter is absolutely a better alternative. Secondly, it is important to include reactive power and harmonics control capability in the PV inverter in a building-integrated project. Previous studies show that the LC-coupling inverter is able to control active power, reactive power, and suppress harmonics simultaneously.

In this paper, a low dc voltage PV generation system with reactive power control and harmonic suppression capability will be developed. It is designed to meet the requirement of small-scale BIPV systems. The available rooftop area for installing PV panels

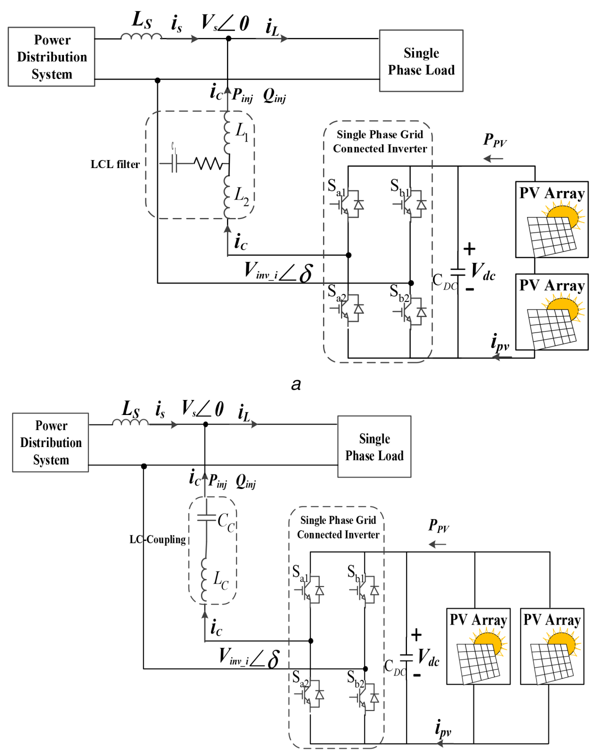

Fig. 1 *Single-stage PV inverter*
(a) LCL coupling and ***(b)*** LC coupling

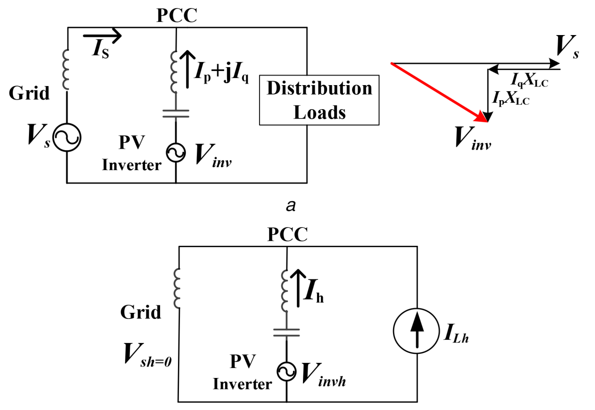

Fig. 2 *Equivalent circuit and vector diagram*
(a) At fundamental frequency ***(b)*** At harmonic frequency

could be very limited due to green areas and other facilities. The proposed LC-coupling PV inverter greatly reduces the minimum number of series-connected PV panels in comparison with a conventional single-stage PV inverter. The main contributions of this paper are as follows:

- Integrate MPPT method to dc-link voltage regulation of an LC-coupling inverter
- Current controller parameter and LC-coupling impedance selection method are deduced based on system response
- A detailed comparison study is provided for the LC-coupling inverter and LCL-coupling inverter.

Section 2 presents the system configuration of the proposed LC-coupling inverter and its basic operation principle. Its control system is given in Section 3, and the parameter design of the LC-coupling PV inverter is further investigated in Section 4. A comparison study between the proposed LC-coupling inverter and conventional LCL-coupling inverter is given in Section 5. Section 6 presents the simulation analysis. A lab-scale prototype is built and tested. Experimental results are provided in Section 7. Finally, Section 8 gives a summary and conclusion.

2 LC-coupling single-stage PV inverter

The system configuration of the LC-coupling PV inverter is shown in Fig. 1*b*, which consists of a dc bus, a full-bridge inverter, and a series LC-coupling branch. In comparison with Fig. 1*a*, the LC branch replaces the LCL filter in a conventional PV integration system.

2.1 Operational principle

The basic function of a PV inverter is to transfer active power from PV panels to the grid. The proposed LC-coupling single-stage PV inverter is designed for the building-integrated system. In order to improve cost effectiveness, the proposed inverter also has the ability of reactive power conditioning and harmonic suppression.

The equivalent circuit and corresponding vector diagram at fundamental frequency are shown in Fig. 2*a*. The equivalent circuit at harmonic frequency is shown in Fig. 2*b*. It is assumed that the grid side is connected to a stiff source with high short circuit capacity such that the harmonic distortion at the grid side voltage can be neglected. Fundamental frequency impedance of the LC-coupling impedance X_{LC} is expressed as

$$X_{\mathrm{LC}} = \frac{1}{\omega C_{\mathrm{C}}} - \omega L_{\mathrm{C}} \tag{1}$$

Therefore, the dc-link voltage can be calculated by

$$V_{\mathrm{dc}} = \sqrt{2} M V_{\mathrm{inv}} = \sqrt{2} M \cdot \sqrt{(V_{\mathrm{s}} - I_{\mathrm{q}} X_{\mathrm{LC}})^2 + (I_{\mathrm{p}} X_{\mathrm{LC}})^2} \tag{2}$$

where I_{p} and I_{q} are active and reactive current injecting to the grid by the PV inverter, respectively. It is assumed that I_{q} is positive when its phase angle leads to the grid-side voltage. The minimum dc-link voltage value can be obtained. A coefficient M is then introduced since the modulation index is not unity in most cases. M needs to be set higher when harmonic compensation is considered. Correspondingly, the relationship between the dc-link voltage and power flow of the PV inverter is expressed by (3), in which P_{inj} and Q_{inj} are active and reactive power injecting to the grid from the PV inverter:

$$V_{\mathrm{dc}} = \sqrt{2} M \cdot V_{\mathrm{s}} \sqrt{\left(1 - \frac{Q_{\mathrm{inj}} X_{\mathrm{LC}}}{V_{\mathrm{s}}^2}\right)^2 + \left(\frac{P_{\mathrm{inj}} X_{\mathrm{LC}}}{V_{\mathrm{s}}^2}\right)^2} \tag{3}$$

2.2 Number of series-connected PV panels

The DC-link voltage of the PV inverter is selected according to the required power control range. However, the dc-link voltage is not fixed in the proposed PV inverter since it is also regulated by the MPPT method, which is important for increasing the efficiency of the PV generation system. In a single-stage PV integration system, series-connected PV panels need to provide the dc voltage, which is high enough for the inverter's operation.

Therefore, the minimum number of series-connected PV panels is estimated by (4) and the obtained value is rounded up to the nearest integer:

$$N_{\mathrm{pv\_series}} \geq V_{\mathrm{dc}} / (K \cdot V_{\mathrm{oc}}) \tag{4}$$

In (4), V_{oc} is the open-circuit voltage of a single PV panel and K is a constant varying between 0.7 and 0.8. The output voltage of the PV panel usually varies inside this range [25]. It can be concluded from (4) that the dc-link voltage plays an important role in determining the number of PV panels. As mentioned before, the LC-coupling inverter is able to operate with its dc-link voltage lower than grid voltage. Hence, less PV panels need to be connected in series by using the proposed inverter. In comparison with an LCL-coupling inverter, the proposed LC-coupling inverter

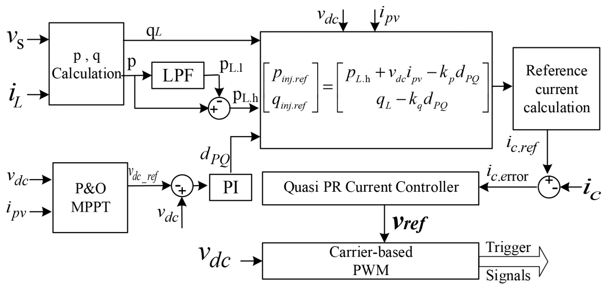

Fig. 3 *Block diagram of the control system*

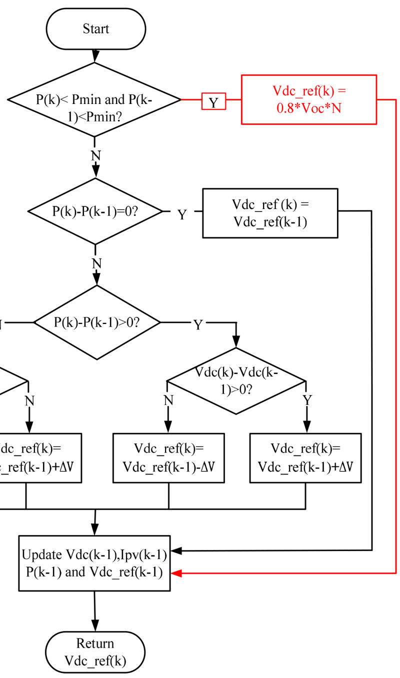

Fig. 4 *Flowchart of dc-link voltage reference determination*

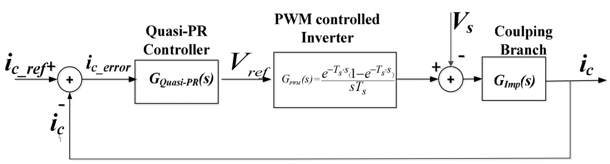

Fig. 5 *Control model block diagram*

allows greater flexibility in configuring PV panels. This makes it a promising alternative in the building-integrated system.

3 Control system

The control block diagram of the proposed LC-coupling PV inverter is shown in Fig. 3, which includes modules for implementing MPPT, dc-link voltage regulation, reference current extraction, and current tracking.

3.1 DC voltage regulation and MPPT

DC voltage regulation plays an important role in PV inverter control, since it maintains the power balance of the whole system. The typical dc-link voltage control involves a PI controller to make dc voltage tracking a pre-set reference. However, the dc-link reference is not fixed in the proposed PV inverter, since MPPT is also achieved by regulating the dc-link voltage. The perturbation and observation method is selected in this work for its simplicity and generic nature [25, 26]. In this method, the power change direction is measured after a perturbation voltage ΔV is added to the dc-link voltage reference. Then, the dc reference is adjusted, so that the dc-link voltage approaches the maximum power point of PV panels. The flowchart of dc-link voltage reference determination is given in Fig. 4, in which V_{dc}, I_{pv}, and P are the dc-link voltage, output current, and power of the PV array, respectively.

In addition, the LC-coupling PV inverter is able to compensate reactive power and harmonics, even though there is no output power from the PV array. In order to keep the inverter operating properly, the dc-link voltage of the inverter is kept at a pre-set value when output power from the PV array is low, as illustrated in Fig. 4.

3.2 Reference signal for inverter control

The LC-coupling single-stage PV inverter extracts maximum active power from the PV array, compensates reactive power, and suppresses harmonics at PCC. From Fig. 3, its output reference power is extracted as follows:

$$\begin{bmatrix} p_{\text{inj.ref}} \\ q_{\text{inj.ref}} \end{bmatrix} = \begin{bmatrix} p_{\text{L}.h} + v_{\text{dc}} i_{pv} - k_p d_{PQ} \\ q_{\text{L}} - k_q d_{PQ} \end{bmatrix} \tag{5}$$

where $p_{\text{L}.\text{h}}$ is the ac component of the instantaneous load active power p_{L}, which corresponds to the load current harmonics. The active power reference also includes power from the PV array. q_{L} is the reactive power of the loads connecting to the PCC. The dc-link voltage regulation of the LC-coupling inverter is done by feeding back control signals to both active and reactive power references but with a different ratio. Single-phase instantaneous reactive power theory is used to calculate reference current from reference power:

$$i_{c\_\text{ref}} = \frac{1}{v^2} [v\sin\theta \quad v\cos\theta] \begin{bmatrix} P_{\text{inj.ref}} \\ Q_{\text{inj.ref}} \end{bmatrix} \tag{6}$$

The inverter's output current is controlled to track the reference computed from (6). As a result, the proposed PV inverter is capable to inject active power for PV generation, reactive power for power factor correction, and harmonics for harmonic suppression to the PCC simultaneously. The current reference and output current of the inverter are sent to a current controller, which generates the reference signal for the pulse width modulation (PWM) controller. The quasi-PR controller is adopted, which is able to reduce the fundamental frequency current tracking error and its transfer function is shown as follows:

$$G_{\text{Quasi\_PR}}(s) = K_{\text{p}} + \frac{2K_{\text{r}}\omega_{\text{c}}s}{s^2 + 2\omega_{\text{c}}s + \omega_0^2} \tag{7}$$

Since the dc-link voltage is not a fixed value in the proposed inverter, it is also sent to the PWM module. The inverter's reference voltage is normalised by V_{dc} before it is compared with the carrier wave. Finally, trigger signals are sent to the single-phase full-bridge inverter.

4 System parameter selection

The control model of the LC-coupling single-stage PV inverter is given in Fig. 5. The overall transfer function is expressed as follows:

$$\begin{aligned} I_c(s) &= G_{ic}(s) I_{c\_\text{ref}}(s) - G_{vs}(s) V_{\text{S}}(s) \\ &= \frac{G_{\text{Quasi-PR}}(s) G_{\text{PWM}}(s) G_{\text{Imp}}(s)}{1 + G_{\text{Quasi-PR}} G_{\text{PWM}}(s) G_{\text{Imp}}(s)} I_{c\_\text{ref}}(s) \\ &\quad - \frac{G_{\text{Imp}}(s)}{1 + G_{\text{Quasi-PR}} G_{\text{PWM}}(s) G_{\text{Imp}}(s)} V_{\text{S}}(s) \end{aligned} \tag{8}$$

The PWM unit is approximated by (9) and the coupling impedance of the LC-coupling inverter is expressed by

$$G_{\text{PWM}}(s) = \frac{\mathrm{e}^{-T_s \cdot s}(1 - \mathrm{e}^{-T_s \cdot s})}{T_s \cdot s} \approx \frac{1 - 0.5 \cdot T_s \cdot s}{(1 + 0.5 \cdot T_s \cdot s)^2} \tag{9}$$

$$G_{\text{Imp}}(s) = G_{\text{LC}}(s) = \frac{C_c s}{L_c C_c s^2 + 1} \tag{10}$$

The performance of the proposed PV inverter is mainly affected by the following factors and more detailed analyses are provided hereinafter.

- Quasi-PR controller design
- LC-coupling impedance selection

4.1 Quasi-PR controller design

The current controller generates the reference voltage of the inverter from the current tracking error. A quasi-PR controller is used, in which K_{p}, K_{r}, and ω_{c} are the three parameters need to be set. ω_{c} is set to minimise the control error at fundamental frequency, so that the active and reactive power of the LC-coupling inverter are accurately controlled.

A higher value for K_{p} is important to reduce the steady-state error. However, this value needs to be bounded by the system stability margin. Once the coupling impedance and sampling frequency of the LCL-coupling inverter are fixed, the root location of its control model is determined by parameters of the PR controller, as illustrated in (8). As a result, the stability margin needs to be considered when the PR controller is designed.

Fig. 6*a* shows the root locus of (8) when K_{p} increases. Although all the roots locate at the left side of the imaginary axis, it is preferred that a stability margin can be kept when a proper value of K_{p} is selected. Fig. 6*b* shows the root locus when K_{r} varies. It is obvious that increasing K_{r} does not affect the system stability. A relatively high value can be selected for K_{r} in a quasi-PR controller.

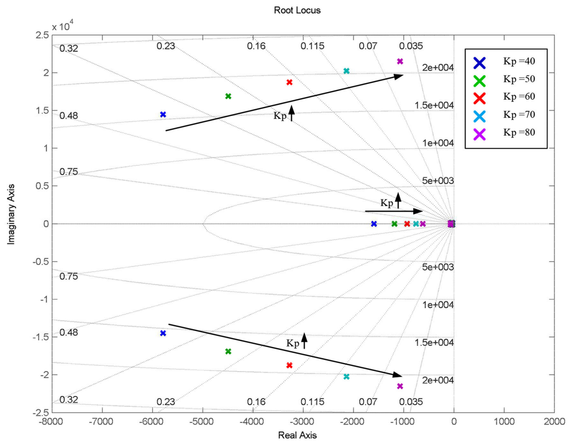

a

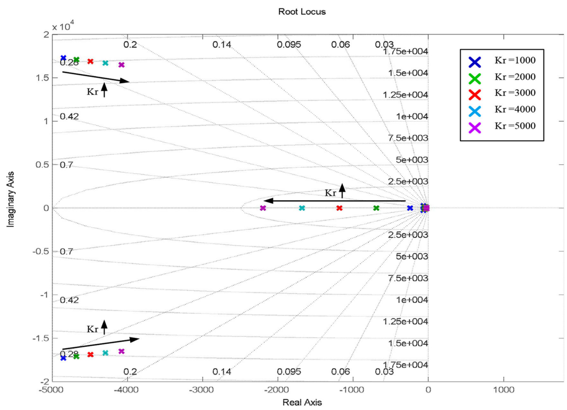

b

Fig. 6 *Root locus of quasi-PR controller*
(a) K_{p} varies and ***(b)*** K_{r} varies

4.2 LC-coupling impedance design

In order to calculate the inductor and capacitor values of the LC branch, two conditions are required. The first one is that the total fundamental frequency impedance of the LC-coupling branch should be capacitive (for inductive loading compensation), which can be calculated in terms of average reactive power injected to the grid [22]. The second condition is obtained from the resonant frequency, as $X_{\text{Lc}} = X_{\text{Cc}}$ at this frequency. By combining the two conditions, we can determine the inductor and capacitor value of an LC-coupling inverter.

The two conditions are expressed as follows:

$$C_c = \frac{1}{(N\omega_f)^2 L_c} \tag{11}$$

$$L_c = \frac{V_s^2}{Q_{\text{average}}(N^2 - 1)\omega_f} \tag{12}$$

where ω is the fundamental frequency and N is the coefficient adjusting resonant frequency of the LC circuit. Next, how to select a proper N value will be investigated.

According to (8), the open-loop and closed-loop system responses of $G_{ic}(s)$ are shown in Fig. 7, in which N is set to 3, 4, 5, 6, and 7, respectively. It is obvious that the frequency response <100 Hz is almost the same for all the curves in Fig. 7. The PR controller is designed to increase the open-loop gain at fundamental frequency, so that the closed loop is unity in the vicinity of 50 Hz. However, the open-loop gain is also extremely high at LC resonant frequency and its position varies in terms of N value. That is to say, the second-order LC-coupling branch is able to improve harmonic current tracking without extra control loops. It can be found from Fig. 7 that a higher LC resonant frequency keeps the closed-loop gain approaching unity with a broader spectrum. There is no need to use multi-PR control loops, which is a common practice for harmonic control in a conventional LCL-coupling inverter.

It seems that it is better to select a higher resonant frequency for the LC circuit. However, the closed-loop gain is amplified at a high-frequency range as shown in Fig. 7. An upper limit is set for $G_{\text{cref\_c}}(s)$ at a high-frequency range. In order to deduce the upper boundary of the resonant frequency coefficient N, $G_{\text{cref\_c}}(s)$ is simplified first by replacing quasi-PR controller with a P controller and by simplifying the PWM unit to $G_{\text{PWM}}(s) = 1 - T_s s$ based on the zero-order Pade′ approximation. As a result, $G_{\text{cref\_c}}(s)$ can be simplified as

$$G_{\text{cref\_c}}(s) = \frac{s^2 - s/T_s}{(1 - L_c/K_p T_s)s^2 - s/T_s - 1 - 1/(C_c K_p T_s)} \tag{13}$$

Since the high-frequency gain is evaluated, e.g. is $> 2\pi \cdot 1000$, (13) can be further simplified to (14) and an upper limit of 10 dB is set:

$$\left| G_{\text{cref\_c}}(s)|_{s = jw} \right| \le \frac{1}{\left| 1 - (L_c/K_p T_s) \right|} \le 10\,\text{dB} \tag{14}$$

Correspondingly, the upper boundary of the resonance frequency order N is expressed as follows:

$$N < \sqrt{1 + \frac{V_S^2}{0.684 \cdot K_p T_s \omega_f \cdot Q_{\text{average}}}} \tag{15}$$

Therefore, (15) provides a method to calculate the upper limit of N. The final N value is selected by rounding down the upper limit to the nearest integer. Next, LC-coupling impedance is obtained by submitting the N value to (11) and (12). In this way, the implemented LC-coupling PV inverter is able to attenuate low-order harmonics of non-linear loads and suppress switching frequency ripples at the same time.

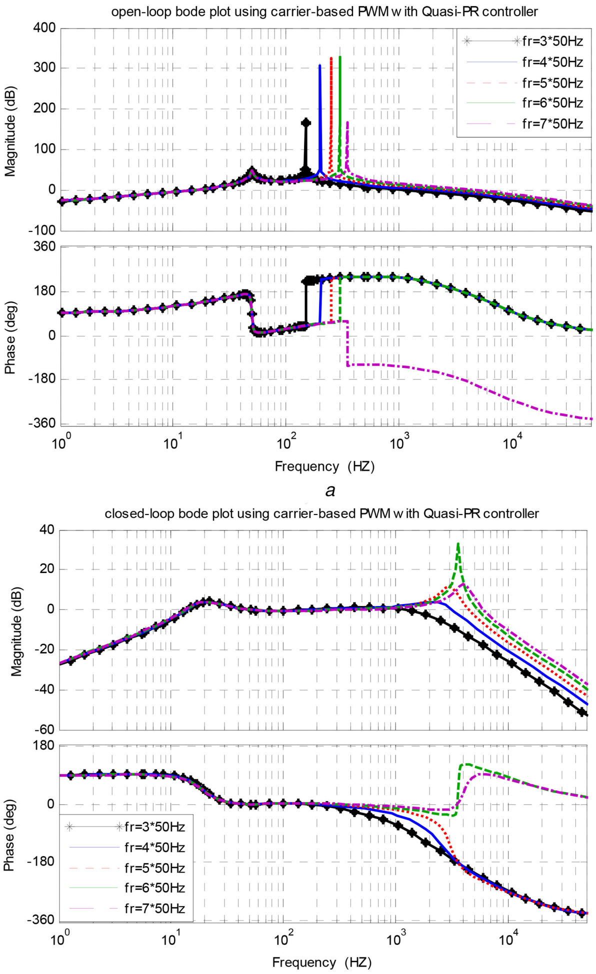

Fig. 7 *System response*
(a) Open loop, ***(b)*** Closed loop

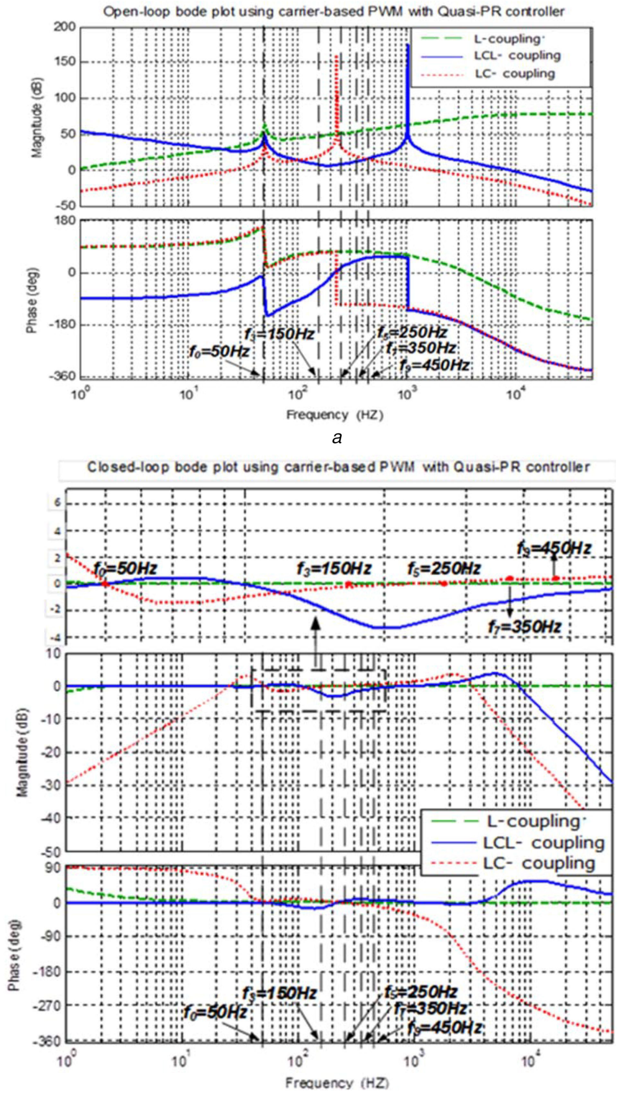

Fig. 8 *System response of PV inverters*
(a) Open loop and ***(b)*** Closed loop

Table 1 Parameters

PV inverter	LCL coupling	LC coupling
PV panels in series	20	10
PV panels in parallel	1	2
coupling impedance	$L_1 = 0.5$ mH	
	$L_2 = 13.5$ mH	$L_c = 3.12$ mH
	$C = 50$ μF	$C_c = 202$ μ
	$R = 12\ \Omega$	
quasi-PR controller	$K_p = 40$	$K_p = 50$
	$K_r = 8400$	$K_r = 5800$
	$\omega_c = 6.28$	$\omega_c = 6.28$
dc-link voltage	around 400 V	around 200 V

5 Comparison between LCL-coupling PV inverter and LC-coupling PV inverter

5.1 Case study

A PV inverter is used to integrate a PV array with 20 panels to a 220 V/50 Hz power distribution system. The coupling impedance, control parameters, and dc-link voltage of the two inverters are listed in Table 1.

It is assumed that the open-circuit voltage of each panel is ∼20 V. Hence, 20 panels are connected in series for a conventional LCL-coupling inverter in Table 1, since its dc-link voltage has to be higher than the grid voltage's peak value. However, the required dc-link voltage of an LC-coupling inverter is cut to half for integrating the same number of PV panels. The PV panels can be configured to two strings when the proposed LC-coupling inverter is used. That is to say, the proposed inverter can be applied to a 10-panel system which does not satisfy the minimum requirement of an LCL-coupling inverter.

5.2 System performance comparison

The current tracking model in Fig. 5 could also be applied to analyse PV inverters using the L filter or LCL filter. Their coupling impedance can be expressed as follows:

$$G_{\mathrm{Imp}}(s) = G_L(s) = \frac{1}{sL_2} \tag{16}$$

$$G_{\mathrm{Imp}}(s) = G_{\mathrm{LCL}}(s) = \frac{1}{s} \cdot \frac{CL_2 s^2 + CRs + 1}{CL_1 L_2 s^2 + CR(L_1 + L_2)s + L_1 + L_2} \tag{17}$$

System responses of an L-coupling inverter, an LCL-coupling inverter, and an LC-coupling inverter are shown in Fig. 8. The PV inverter using the L filter is not able to attenuate high-frequency components. Both LCL-coupling inverter and the proposed LC-coupling are able to attenuate high-frequency ripples.

In addition, the low-frequency region of the system response is enlarged and is shown in Fig. 8*b*. The proposed LC-coupling inverter keeps its current tracking error low at dominant low-order harmonics, e.g. third, fifth, and seventh harmonics. As shown in Fig. 8, the harmonics compensation performance of the LC-coupling inverter is better than that of the LCL-coupling inverter as

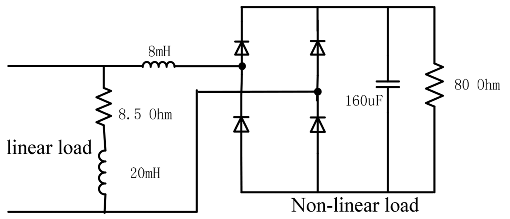

Fig. 9 *Load model*

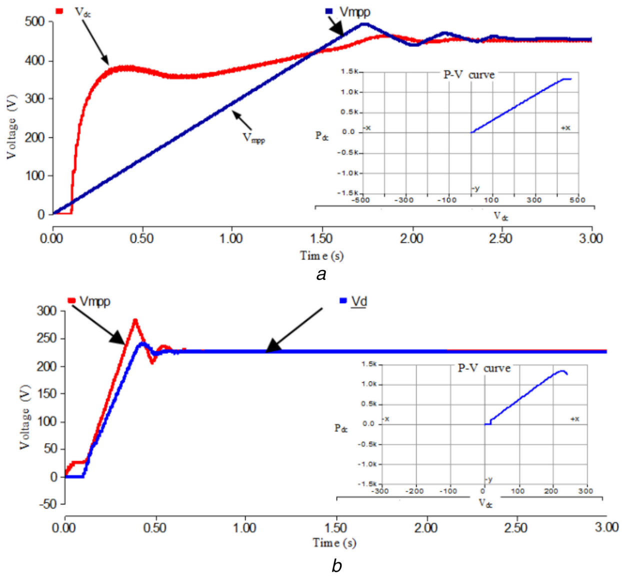

Fig. 10 *DC-link voltage regulation for MPPT*
(a) LCL-coupling PV inverter, ***(b)*** LC-coupling PV inverter

harmonic contents can be further suppressed. In summary, the proposed LC-coupling inverter obtains the following advantages in comparison with an LCL-coupling inverter.

- Uses less coupling components
- Performs better in low-order harmonics compensation without extra PR control loops
- No active or passive resonant damping is required

In addition, since the proposed LC-coupling inverter can operate under a dc-link voltage lower than the grid voltage, this allows more flexibility in PV panels' configuration. This characteristic is favourable especially for small-capacity building-integrated projects.

6 Simulation results

6.1 System configuration and parameters

Simulation models are built by using PSCAD™/EMTDC™. Both LCL-coupling PV inverter and LC-coupling PV inverter are implemented. The system configuration is shown in Fig. 1 and its control system is shown in Fig. 3. The system parameters are listed in Table 1. Both linear load and non-linear loads are connected to the PCC. The load model is shown in Fig. 9. One group of load parameters are also given in Fig. 9.

6.2 Comparison between LCL-coupling inverter and LC-coupling inverter

The comparison between the LCL-coupling inverter and LC-coupling inverter is carried out. The single-stage PV inverter is controlled to track the maximum power point, transfer the active power to the gird, and compensate reactive power and current harmonics of the loads simultaneously. A PV module is used in the simulation to test the proposed dc voltage regulation with MPPT.

The MPPT and dc-voltage regulation results are shown in Fig. 10, in which V_{dc} denotes the dc-link voltage, and V_{mpp} is the dc-link voltage reference generated by the MPPT module. From the P–V curves, both PV inverters are able to track the maximum power point. However, the steady-state dc-link voltage of the LC-coupling PV inverter is about half of that of the LCL-coupling PV inverter. It also takes less time to reach the maximum power point. At the same time, the dc voltage ripple is smaller as less PV panels are connected in series. The grid voltage, dc-link voltage, source current, load current, and source current total harmonic distortion (THD) are shown in Fig. 11.

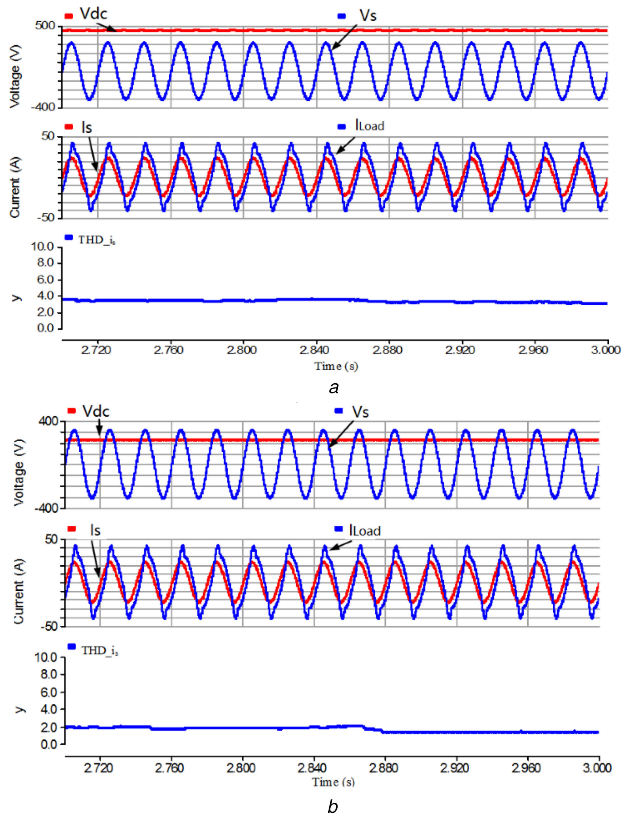

Fig. 11 *Waveforms of grid voltage, dc-link voltage, source current, load currents, and source current THD results*
(a) LCL-coupling PV inverter, ***(b)*** LC-coupling PV inverter

Table 2 Simulation results

	THD	Power factor	Active power of PV
before compensation	15.94%	0.86	NA
LCL-coupling inverter	3.07%	1.0	1195.27 W
LC-coupling inverter	1.35%	1.0	1225.68 W

The power factor at the grid side, THD of the source current, and output active power are measured and summarised in Table 2. Both PV inverters inject active power to the PCC. The harmonics in the source side is compensated by the PV inverter. Hence, its THD value is greatly reduced. The power factor at the source side is also corrected to 1 by the PV inverter. In addition, the LC-coupling single-stage PV inverter achieves the pre-set target with a lower dc-link voltage, and its performance in current harmonic attenuation is better.

6.3 Simulation verification of the LCL-coupling inverter

The dynamic response of the LCL-coupling inverter is tested. The inverter output power and its dc-link voltage variations are shown in Figs. 12 and 13. In Fig. 12, P_{dc} is the PV panel output active power and P_{inj} indicates the active power being injected to the unity gird. Q_{load} and Q_{inj} are the load side reactive power and reactive power from the PV inverter, respectively. The irradiation level of the PV module is set higher at 2 s. The active power being injected to the PCC increases accordingly. The load reactive power

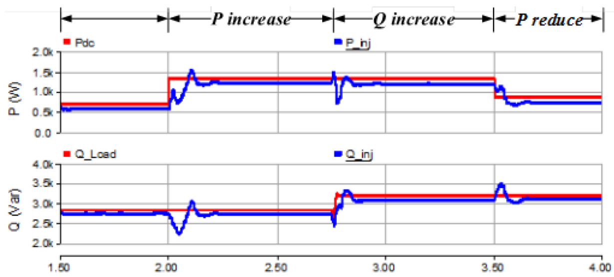

Fig. 12 *Active power and reactive power*

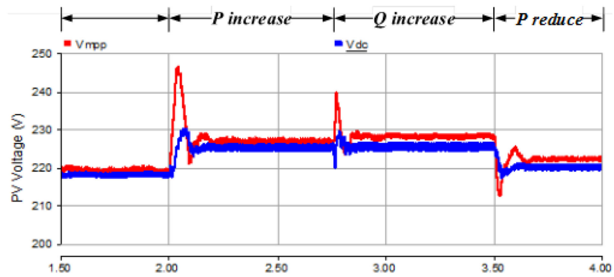

Fig. 13 *DC-link voltage variation*

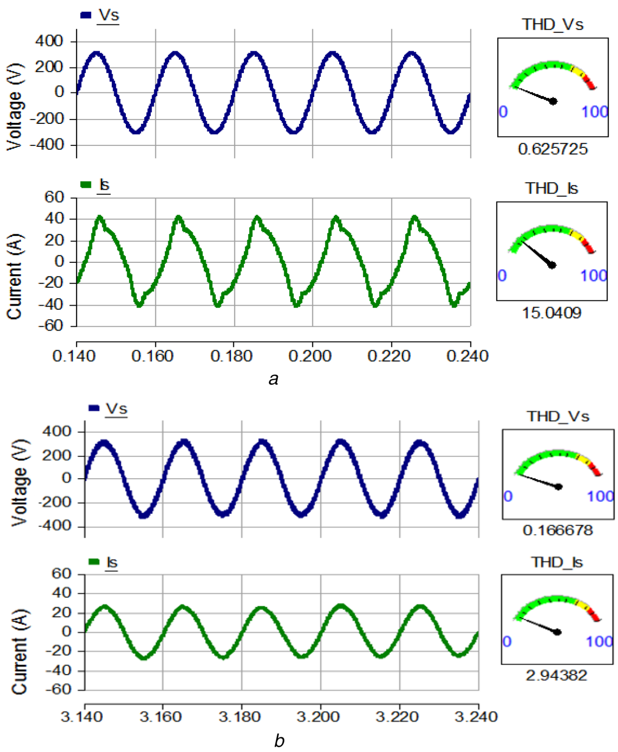

Fig. 14 *Voltage, current and their THD values*
(a) Without LC-coupling inverter *(b)* With LC-coupling inverter

consumption increases at 2.75 s and the solar irradiation level is set lower at 3.0 s.

An ideal ac source is used in simulation. However, the voltage at PCC is distorted when the load current contains harmonics. The THD of the voltage at PCC is measured with and without the LC-coupling PV inverter when the non-linear load is connected. The voltage at PCC and the grid side currents are shown in Fig. 14. Results indicate that the THD of the voltage decreases after current harmonics are compensated by the LC-coupling PV inverter.

7 Experimental results

A laboratory-scale experimental LC-coupling PV inverter prototype was built. The photo of the experimental platform and prototype is shown in Fig. 15. The system parameters are listed in Table 3. Due to the power capacity of the laboratory, the grid side

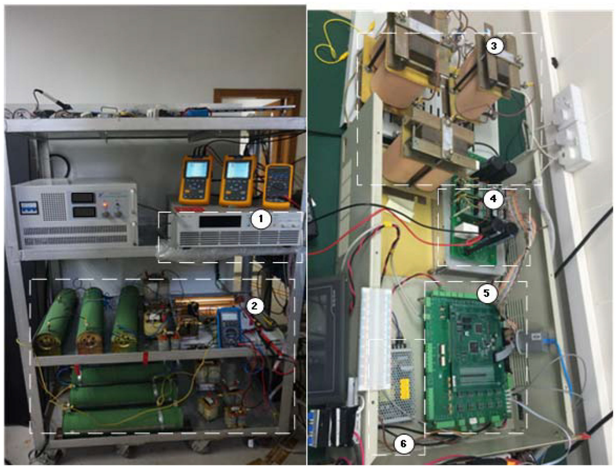

Fig. 15 *Experimental prototype*
① – Programmable DC power supply; ② – Loads; ③ – LC impedance; ④ – IGBT driver; ⑤ – Control board and signal conditional circuit; ⑥ – Power supply for control circuit

Table 3 Experimental prototype parameters

Parameters	Value
grid voltage VS	110 Vrms, 50 Hz
switching frequency fs	10 kHz
sampling frequency	20 kHz
power base	560 Var
inductor L_C	3.79 mH
capacitor C_C	140 μF

voltage is decreased to 110 V. The control system is based on the DSP TMS320F28335. The PV output is generated by a programmable dc power supply (Chroma 62100H-600S), which is able to simulate the output characteristics of the PV array, so that the MPPT function of the PV inverter could be tested.

The LC-coupling PV inverter is used to achieve MPPT, inject active power to the grid, compensate reactive power, and suppress the harmonics of the non-linear load. The dc-link voltage is ∼80 V and the voltage at the PCC is 110 V. The LC-coupling single-stage PV inverter is able to reduce the inverter operational voltage. The experimental results are shown in Fig. 16 and summarised in Table 4.

Fig. 16*a* is the P–V curve captured from the programmable dc power supply. The red point is located by the output voltage and power of the dc power supply. It is shown in Fig. 16*a* that the operational point locates near the maximum power point.

Voltage, current, and harmonic spectrum are recorded before PCC (grid side), after PCC (load side), and at output of the PV inverter. Results are shown in Fig. 16*b*. The source current distortion is reduced to 3.3% from the original 18.3%, and the power factor can be improved to 0.99 from 0.83. Moreover, the PV inverter can inject the active power of 115 W, which is close to the PV panel's maximum output of 130 W.

8 Conclusion

The comprehensive design and control of a multi-functional LC-coupling PV inverter with low dc-link voltage characteristics is studied in this paper, which can reduce the system's initial cost and operational cost. The proposed inverter is a promising alternative to the existing PV inverter, since it reduces the minimum number of PV panels for a single array. This provides more flexibility in the PV panel configuration in a building-integrated system. The effect of shading condition on the output of the PV panel array generation can be alleviated since less panels are connected per string. The dc voltage regulation with MPPT and coupling impedance design are studied. The control of the proposed inverter is simpler than that of the conventional LCL-coupling PV inverter. Simulation verifications and experimental tests are provided to

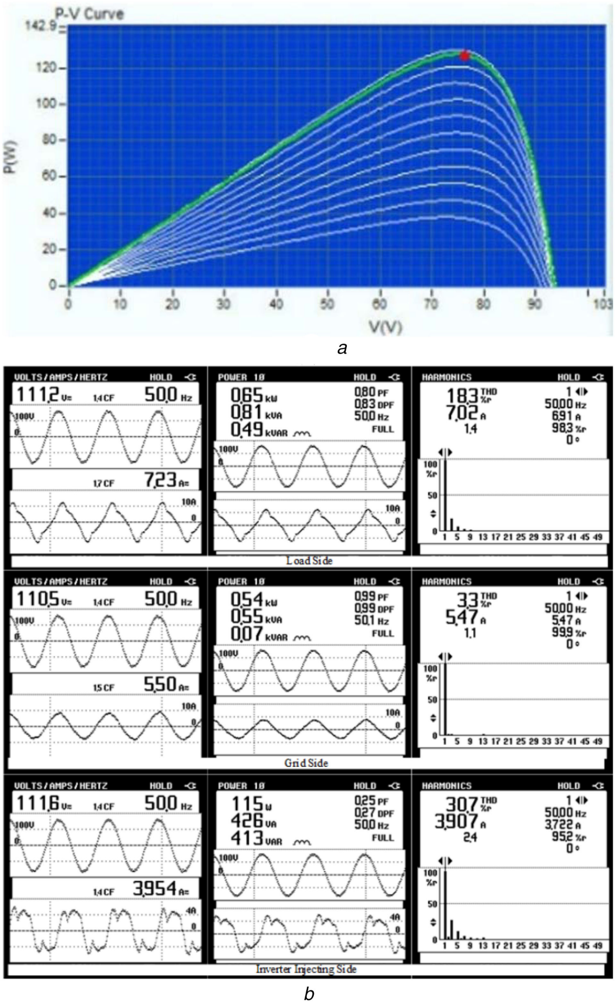

Fig. 16 *Experimental results*
(a) MPPT and ***(b)*** Voltage, current and THD recorded at load side, grid side, and inverter output side

Table 4 Experimental results

	Load side	Source side
power factor	0.83	0.99
current THD	18.3%	3.3%
injected active power	N/A	115 W

validate the effectiveness of the proposed PV inverter and its control.

9 Acknowledgments

The authors would like to thank University of Macau for financial support of projects (MYRG2018-00097-FST and MYRG2015-00084-FST) and the Science and Technology Development Fund, Macao SAR Government for financial support of project (072/2012/A3).

10 References

[1] Palmer, D., Koubli, E., Cole, I., *et al.*: 'Comparison of solar radiation and PV generation variability: system dispersion in the UK', *IET Renew. Power Gener.*, 2017, **11**, (5), pp. 550–557

[2] Watson, J., Watson, N., Santos-Martin, D., *et al.*: 'Impact of solar photovoltaics on the low-voltage distribution network in New Zealand', *IET Gener. Transm. Distrib.*, 2016, **10**, (1), pp. 1–9

[3] Hu, K., Li, W., Wang, L., *et al.*: 'Topology and control strategy of power optimisation for photovoltaic arrays and inverters during partial shading', *IET Gener. Transm. Distrib.*, 2018, **12**, (1), pp. 62–71

[4] https://www.cem-macau.com/en/customer-service/tariff-information/tariff-group-b/

[5] Jose, D., Gounden, N., Ravishankar, J.: 'Simple power electronic controller for photovoltaic fed grid-tied systems using line commutated inverter with fixed firing angle', *IET Power Electron.*, 2014, **7**, (6), pp. 1424–1434

[6] Wolfs, P.: 'A review of the single phase photovoltaic module integrated converter topologies with three different DC link configurations', *IEEE Trans. Power Electron.*, 2008, **23**, (3), pp. 1320–1333

[7] Kjaer, S., Pedersen, J., Blaabjerg, F.: 'A review of single-phase grid-connected inverters for photovoltaic modules', *IEEE Trans. Ind. Appl.*, 2005, **41**, (5), pp. 1292–1306

[8] Wu, T., Chang, C., Lin, L., *et al.*: 'Power loss comparison of single- and two-stage grid-connected photovoltaic systems', *IEEE Trans. Energy Convers.*, 2011, **26**, (2), pp. 707–715

[9] Reiter, R., Oliveira, S., Peres, A., *et al.*: 'Digital resonant controller for dual-stage photovoltaic inverter system with small dc-bus capacitor', *IET Power Electron.*, 2016, **9**, (6), pp. 1315–1321

[10] Jain, C., Singh, B.: 'Single-phase single-stage multifunctional grid interfaced solar photo-voltaic system under abnormal grid conditions', *IET Gener. Transm. Distrib.*, 2015, **9**, (10), pp. 886–894

[11] Rajan, S., Vengatesh, R.: 'Investigation of the effects of homogeneous and heterogeneous solar irradiations on multicrystal PV module under various configurations', *IET Renew. Power Gener.*, 2015, **9**, (3), pp. 245–254

[12] Wang, X., Blaabjerg, F., Loh, P.: 'Virtual RC damping of LCL-filtered voltage source converters with extended selective harmonic compensation', *IEEE Trans. Power Electron.*, 2015, **30**, (9), pp. 4726–4737

[13] Xin, Z., Loh, P., Wang, X., *et al.*: 'Highly accurate derivatives for LCL-filtered grid converter with capacitor voltage active damping', *IEEE Trans. Power Electron.*, 2016, **31**, (5), pp. 3612–3625

[14] Park, S., Chen, C., Lai, J.: 'A wider-range active and reactive power flow controller for a solid oxide fuel cell power conditioning system', *IEEE Trans. Power Electron.*, 2008, **23**, (6), pp. 2703–2710

[15] Xiao, F., Dong, L., Liao, X.: 'Fast reactive current detection method for single-phase grid-connected inverters', *IET Power Electron.*, 2016, **9**, (3), pp. 401–407

[16] Ibrahim, S., Cramer, A., Liu, X., *et al.*: 'PV inverter reactive power control for chance-constrained distribution system performance optimisation', *IET Gener. Transm. Distrib.*, 2018, **12**, (5), pp. 1089–1098

[17] Castilla, M., Miret, J., Matas, J., *et al.*: 'Control design guidelines for single-phase grid-connected photovoltaic inverters with damped resonant harmonic compensators', *IEEE Trans. Ind. Electron.*, 2009, **56**, (11), pp. 4492–4501

[18] Shen, G., Zhu, X., Zhang, J., *et al.*: 'A new feedback method for PR current control of LCL-filter-based grid-connected inverter', *IEEE Trans. Ind. Electron.*, 2010, **57**, (6), pp. 2033–2041

[19] Wu, W., Liu, Y., He, Y., *et al.*: 'Damping methods for resonances caused by LCL-filter-based current-controlled grid-tied power inverters: an overview', *IEEE Trans. Ind. Electron.*, 2017, **64**, (9), pp. 7402–7413

[20] Giacomini, J., Michels, L., Pinheiro, H., *et al.*: 'Design methodology of a passive damped modified LCL filter for leakage current reduction in grid-connected transformerless three-phase PV inverters', *IET Renew. Power Gener.*, 2017, **11**, (14), pp. 1769–1777

[21] Wang, X., Pang, Y., Loh, P., *et al.*: 'A series-LC-filtered active damper with grid disturbance rejection for AC power-electronics-based power systems', *IEEE Trans. Power Electron.*, 2015, **30**, (8), pp. 4037–4041

[22] Dai, N., Zhang, C., Wong, M., *et al.*: 'Analysis, control and experimental verification of a single-phase capacitive-coupling grid-connected inverter', *IET Power Electron.*, 2014, **8**, (5), pp. 770–782

[23] Inzunza, R., Akagi, R.: 'A 6.6-kV transformerless shunt hybrid active filter for installation on a power distribution system', *IEEE Trans. Power Electron.*, 2005, **20**, (4), pp. 893–900

[24] Rajan, S., Vengatesh, R.: 'Investigation of the effects of homogeneous and heterogeneous solar irradiations on multicrystal PV module under various configurations', *IET Renew. Power Gener.*, 2015, **9**, (3), pp. 245–254

[25] Bendib, B., Belmili, H., Krim, F.: 'A survey of the most used MPPT methods: conventional and advanced algorithms applied for photovoltaic systems', *Renew. Sustain. Energy Rev.*, 2015, **45**, pp. 637–648

[26] Kadri, R., Gaubert, J.-P., Champenois, G.: 'An improved maximum power point tracking for photovoltaic grid-connected inverter based on voltage-oriented control', *IEEE Trans. Ind. Electron.*, 2011, **58**, (1), pp. 66–75